JACC: CARDIOVASCULAR INTERVENTIONS VOL. 6, NO. 3, 2013

ISSN 1936-8798/$36.00
PUBLISHED BY ELSEVIER INC. http://dx.doi.org/10.1016/j.jcin.2012.09.017

Optical Coherence Tomography Versus Intravascular Ultrasound to Evaluate Coronary Artery Disease and Percutaneous Coronary Intervention

Hiram G. Bezerra, MD, PhD,* Guilherme F. Attizzani, MD,* Vasile Sirbu, MD,† Giuseppe Musumeci, MD,† Nikoloz Lortkipanidze, MD,† Yusuke Fujino, MD,* Wei Wang, MS,* Sunao Nakamura, MD, PhD,‡ Andrej Erglis, MD,§‖ Giulio Guagliumi, MD,† Marco A. Costa, MD, PhD*

Cleveland, Ohio; Bergamo, Italy; Chiba, Japan; and Riga, Latvia

Objectives We compared intravascular ultrasound (IVUS) and 2 different generations of optical coherence tomography (OCT)—time-domain OCT (TD-OCT) and frequency-domain OCT (FD-OCT)—for the assessment of coronary disease and percutaneous coronary intervention (PCI) using stents.

Background OCT is a promising light-based intravascular imaging modality with higher resolution than IVUS. However, the paucity of data on OCT image quantification has limited its application in clinical practice.

Methods A total of 227 matched OCT and IVUS pull backs were studied. One hundred FD-OCT and IVUS pull backs in nonstented (n = 56) and stented (n = 44) vessels were compared. Additionally, 127 matched TD-OCT and IVUS images were compared in stented vessels.

Results FD-OCT depicted more severe native coronary disease than IVUS; minimal lumen area (MLA) was 2.33 ± 1.56 mm^2 versus 3.32 ± 1.92 mm^2, respectively ($p < 0.001$). Reference vessel dimensions were equivalent between FD-OCT and IVUS in both native and stented coronaries, but TD-OCT detected smaller reference lumen size compared with IVUS. Immediately post-PCI, in-stent MLAs were similar between FD-OCT and IVUS, but at follow-up, both FD-OCT and TD-OCT detected smaller MLAs than did IVUS, likely due to better detection of neointimal hyperplasia (NIH). Post-PCI malapposition and tissue prolapse were more frequently identified by FD-OCT.

Conclusions FD-OCT generates similar reference lumen dimensions but higher degrees of disease severity and NIH, as well as better detection of malapposition and tissue prolapse compared with IVUS. First-generation TD-OCT was associated with smaller reference vessel dimensions compared with IVUS. (J Am Coll Cardiol Intv 2013;6:228–36) © 2013 by the American College of Cardiology Foundation

From the *Harrington Heart and Vascular Institute, University Hospitals Case Medical Center, Case Western Reserve University, Cleveland, Ohio; †Division of Cardiology, Cardiovascular Department, Ospedali Riuniti di Bergamo, Bergamo, Italy; ‡Department of Cardiology, New Tokyo Hospital, Chiba, Japan; §Latvian Centre of Cardiology, Paul Stradins Clinical University Hospital, Riga, Latvia; and the ‖Institute of Cardiology, University of Latvia, Riga, Latvia. Dr. Bezerra has received consulting fees and honoraria from St. Jude Medical, Inc; Dr. Attizzani has received consulting fees from St Jude Medical, Inc.; Dr. Sirbu has received research funding from St. Jude Medical, Inc.; Dr. Guagliumi has received consulting fees from St. Jude Medical, Inc., Boston Scientific, and Volcano, and grant support from St. Jude Medical, Inc., Medtronic Vascular, LightLab Imaging, Boston Scientific, and Abbott Vascular; Dr. Costa has received consulting fees from St. Jude Medical, Inc., Medtronic, Scitech, Cordis, Boston Scientific, and Abbott Vascular. All other authors have reported that they have no relationships relevant to the contents of this paper to disclose. The first 2 authors contributed equally to this paper.

Manuscript received June 28, 2012; revised manuscript received September 6, 2012, accepted September 27, 2012.

Intravascular imaging has helped shape our understanding of coronary artery disease and percutaneous coronary intervention (PCI) (1–5). In particular, intravascular ultrasound (IVUS) contributed significantly to modern PCI techniques (6–8). The recent introduction of optical coherence tomography (OCT) into the catheterization laboratory was received with great expectation, as this light-based imaging modality offers 10 times higher resolution and 40 times faster imaging acquisition compared with IVUS. However, the first-generation time-domain OCT (TD-OCT) (M2CV OCT Imaging System, LightLab Imaging, Westford, Massachusetts) was plagued with the requirement for proximal vessel occlusion to create a blood-free imaging environment. Besides the technical challenges with image acquisition, preliminary studies suggested an underestimation of lumen dimensions by TD-OCT as compared with IVUS (9,10).

More recently, frequency-domain OCT (FD-OCT) (C7XR Imaging System, LightLab Imaging) was developed to overcome the inherent technical limitations of TD-OCT while preserving and potentially improving image quality (11). FD-OCT and IVUS measurements showed good agreement in phantom models (12), but in vivo comparative studies between these commercially available technologies are lacking. Therefore, the present study was designed to provide comparative data between IVUS versus both generations of OCT technologies for the assessment of human coronary artery disease and PCI.

Methods

The study population comprises patients enrolled in different clinical trials that were analyzed in the Cardiovascular Imaging Core Laboratory, University Hospitals Case Medical Center, Cleveland, Ohio. Matched OCT and IVUS images of the native coronary artery immediately post-procedure and 6 to 12 months after stenting were included. The indication for using both imaging modalities was based on study protocols and was approved by the ethics committee of each institution. The inclusion criteria consisted of completeness of the pull back and good image quality as defined by >70% of analyzable frames in both modalities. Exclusion criteria included bifurcation segments in which the side branch occupied more than 45° of the cross section in order to avoid tracing interpolation when quantifying lumen, impossibility of matching IVUS and OCT pull backs for the same patient and time point, and poor or incomplete image availability not fulfilling the inclusion criteria. Patients gave written consent that was approved by the local ethical committee. Patient data were anonymized, and core laboratory analysts were blinded to patient and procedural characteristics.

Imaging acquisition. INTRAVASCULAR ULTRASOUND. IVUS imaging was performed after intracoronary injection of nitroglycerin (100 to 200 μg) using a 40-MHz Atlantis SR Pro catheter (Boston Scientific, Fremont, California). IVUS imaging was carried out with motorized pull back at 1 mm/s to include the target lesion and at least 5 mm proximal and distal as references. All IVUS data were digitally stored for offline analysis.

OPTICAL COHERENCE TOMOGRAPHY. OCT imaging was performed after injection of nitroglycerin (100 to 200 μg). Two different systems were used: TD-OCT (M2CV Imaging System, LightLab Imaging) and FD-OCT (C7XR Imaging System, LightLab Imaging). TD-OCT was performed by the occlusive technique for optimization of blood clearance as described previously (13). FD-OCT was performed with a 2.7-F OCT catheter (Dragonfly imaging catheter, LightLab Imaging), and blood clearance was achieved by nondiluted iodine contrast injection at rates of 3 to 5 ml/s for a total volume of 10 to 20 ml/pull back. Images were acquired with an automated pull back at a rate of 1 mm/s for TD-OCT and 20 mm/s for FD-OCT. Images were digitally stored and submitted for offline evaluation at the core laboratory.

Imaging analysis. All cross-sectional images (frames) were initially screened for quality assessment and excluded from analysis if any portion of the image was out of the screen or the image had poor quality caused by artifacts. In the case of OCT, frames were also excluded if inadequate blood clearance was identified, as defined by the inability to visualize lumen contour in more than 45° (1 quadrant) of the cross section. IVUS and OCT data were analyzed in a similar fashion utilizing validated software. IVUS measurements were obtained by using a computer-based contour detection program (QIvus, Medis Medical, Leiden, the Netherlands). A dedicated semiautomated contour-detection system (OCT system software B.0.1, LightLab Imaging), developed in collaboration with the University Hospitals Imaging Core Laboratory was used for OCT measurements.

Abbreviations and Acronyms

FD-OCT = frequency-domain optical coherence tomography
IVUS = intravascular ultrasound
MLA = minimal lumen area
NIH = neointimal hyperplasia
OCT = optical coherence tomography
PCI = percutaneous coronary intervention
TD-OCT = time-domain optical coherence tomography

CORONARY ARTERY DISEASE ASSESSMENT. In nonstented arteries, the region of interest was selected based on anatomic landmarks (i.e., side branches, calcification) helped by angiographic images containing the IVUS and OCT catheter position. The diseased segment (lesion location) was identified, and the references were defined as the most "normal-appearing" segments 5 mm proximal and distal to the lesion shoulders by OCT and co-registered IVUS. Luminal areas and diameters were assessed at 0.2-mm intervals. Two experienced analysts evaluated the images. In case of discordance between analysts, a third reader was used to reach

a consensus on image matching and quality. Percent area and diameter stenosis were calculated as follows: reference lumen area − minimal lumen area (MLA)/reference lumen area × 100 and reference lumen diameter − MLA/reference lumen diameter × 100, respectively.

POST-PCI AND FOLLOW-UP ASSESSMENTS. Matched stented segments were defined at post-procedure and follow-up FD-OCT and IVUS images, whereas matched stented segments were defined in follow-up TD-OCT and IVUS images utilizing stent edges as landmarks. Lumen and stent cross-sectional areas were traced at 1-mm intervals in both OCT systems and IVUS images. The cross-sectional areas and associated volumes were determined for the stent, lumen, and neointimal area (follow-up images only). Malapposition was qualitatively defined by IVUS as regions containing blood speckle behind the stent. OCT-derived malapposition values were obtained by 360° chords, distributed between the lumen and stent contours as previously described (14). The data were imported to a proprietary database that automatically defines the threshold for malapposition according to the different stent types and accounting for individual strut thickness (15). Tissue protrusion was defined as occurring between stent struts, which directly correlates with the underlying plaque, without abrupt transition or different optical or ultrasound properties (16). Luminal areas and diameters were also obtained at the reference segment, in which cross sections were selected every 1 mm within the 5-mm distal and proximal stent edges. The reproducibility of the applied methodology has been previously reported (17).

Statistics. Data analysis was conducted using SAS Version 9.2 (SAS Institute, Cary, North Carolina). Categorical variables are presented as counts and percentages, and continuous variables are presented as mean ± SD. Comparisons between 3 groups were made using 1-way analysis of variance, with Tukey's post hoc test for the 3 individual-group differences. Differences between IVUS and each OCT technology were evaluated by paired *t* test or a generalized estimating equations model with an exchangeable correlation structure to account for multiple values within the same subject and further examined by Bland-Altman plots. Comparison results were further confirmed with nonparametric Wilcoxon matched-pairs signed rank analysis. The agreement to identify malapposition cases with IVUS versus the OCT method was quantified using Kappa statistics. The correlation between 2 continuous variables was analyzed by simple linear regression with a 95% confidence interval or mixed effects model for repeated measurement, and the nonparametric Mann-Whitney *U* test was used for comparison of malapposition quantitative measurements between OCT and IVUS.

Results

Two hundred twenty-seven IVUS pull backs were matched with 100 FD-OCT (56 native coronary arteries, 26 post-

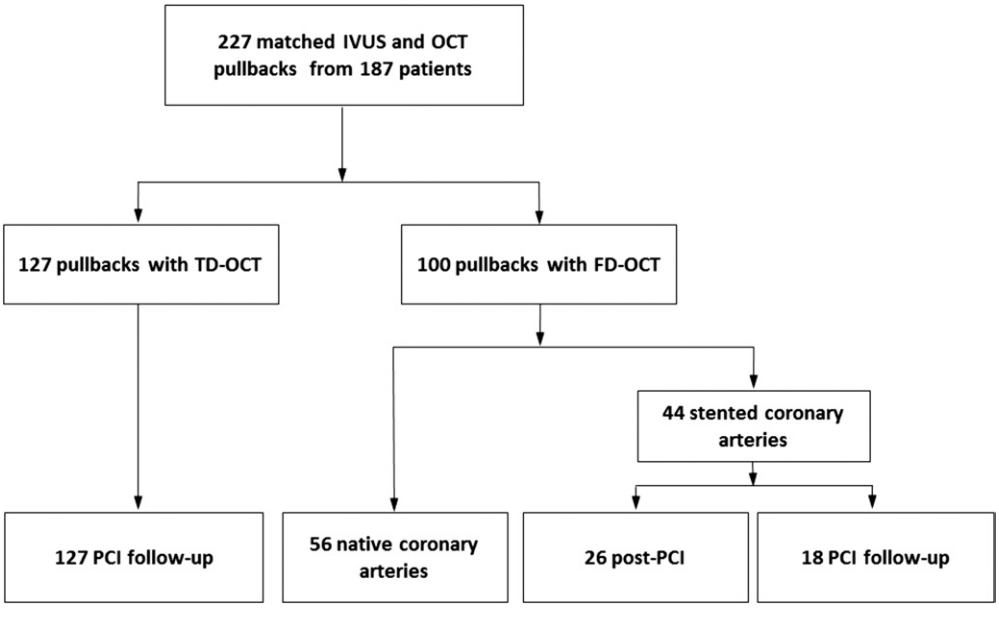

Figure 1. Study Population

FD-OCT = frequency-domain optical coherence tomography; IVUS = intravascular ultrasound; OCT = optical coherence tomography; PCI = percutaneous coronary intervention; TD-OCT = time-domain optical coherence tomography.

Table 1. Demographics and Clinical Characteristics

N	187
Age, yrs	65.1 ± 9.3
Men	145 (77.5)
Diabetes	58 (31.0)
Insulin dependent	5 (8.6)
Hypertension	97 (51.9)
Hypercholesterolemia	101 (54.0)
Chronic renal failure	11 (5.9)
Current smoker	77 (41.2)
Previous MI	31 (16.6)
Peripheral artery disease	13 (7.0)
Stable angina	89 (47.6)
Acute coronary syndrome	37 (19.8)
ST-segment elevation MI	45 (24.1)

Values are mean ± SD or n (%).
MI = myocardial infarction.

PCI, and 18 PCI follow-up) and 127 TD-OCT PCI follow-up images from 187 patients (Fig. 1). Patient demographics are summarized in Table 1.

Coronary artery disease assessment. FD-OCT detected smaller MLAs and diameters (2.33 ± 1.56 mm^2 vs. 3.32 ± 1.92 mm^2, and 1.62 ± 0.48 mm vs. 1.99 ± 0.51 mm, respectively, $p < 0.001$ for both comparisons). Mean reference lumen areas and diameters were equivalent between methods (Table 2, Fig. 2).

Post-PCI assessment of stented vessels. REFERENCE VESSEL. Reference lumen dimensions were comparable between FD-OCT and IVUS (Table 3, Fig. 2).

STENTED SEGMENT. Measurements of in-stent lumen dimensions were equivalent between FD-OCT and IVUS, whereas mean stent area was smaller in FD-OCT (Table 3, Fig. 2). Tissue protrusion and malapposition areas were significantly larger by FD-OCT when compared with IVUS (Table 3). Acute malapposition rates with FD-OCT were 96.2% (25 of 26) versus 42.3% (11 of 26) with IVUS (Kappa: 0.241 [$p < 0.001$]).

Follow-up assessment of stented vessels. REFERENCE VESSEL. As observed in nonstented native coronaries, measurements of reference lumen dimensions were similar between FD-OCT and IVUS (Table 3). However, TD-OCT detected smaller reference lumen dimensions compared with IVUS (Online Table 1).

STENTED SEGMENT. Measurements of the stent were similar, but mean and MLA were smaller by FD-OCT compared with IVUS. More neointimal hyperplasia (NIH) was detected by FD-OCT (Fig. 2, Table 3). Similar results were observed when comparing TD-OCT and IVUS (Online Table 1). IVUS underestimation as compared with that of FD-OCT was more significant at smaller levels of NIH (Online Fig. 1). Overall, combining both OCT systems, late malapposition was demonstrated in 33.1% (48 of 145) of the cases versus 9.7% (14 of 145) by IVUS (Kappa: 0.057 [$p = 1.000$]) at follow-up. Correlations between measurements obtained by both OCT systems and IVUS are represented in Online Figure 2.

Discussion

This report provides the first large comparative data between the 2 clinically available OCT technologies versus matched IVUS images in human coronary arteries. The results showed equivalence between FD-OCT imaging and IVUS to determine coronary reference lumen dimensions, an important metric used in routine PCI. FD-OCT detected more severe disease, smaller MLA, and higher percent stenosis than IVUS. The present data also expand upon prior preliminary observations (10) and confirm, in a large sample, the risk of underestimating reference vessel dimensions when using first-generation TD-OCT with occlusive technique (Online Table 1). The study also demonstrates the higher sensitivity of both OCT systems compared with IVUS to detect stent malapposition, NIH, and intrastent tissue protrusion (Figs. 3 and 4, Online Fig. 3).

Table 2. FD-OCT Versus IVUS Assessment of Native Coronary Artery Disease

	FD-OCT vs. IVUS			
	IVUS (n = 56)	FD-OCT (n = 56)	Difference (OCT—IVUS) (n = 56)	p Value*
Reference lumen area, mm^2	6.45 ± 2.48	6.26 ± 2.33	−0.19 ± 1.16	0.294
Reference lumen diameter, mm	2.82 ± 0.50	2.77 ± 0.50	−0.05 ± 0.26	0.226
Minimal lumen area, mm^2	3.32 ± 1.92	2.33 ± 1.56	−0.99 ± 0.77	<0.001
Minimal lumen diameter, mm	1.99 ± 0.51	1.62 ± 0.48	−0.37 ± 0.25	<0.001
Area stenosis, %	58.47 ± 11.87	71.97 ± 11.22	13.51 ± 10.54	<0.001
Diameter stenosis, %	35.24 ± 9.65	47.98 ± 10.59	12.74 ± 9.60	<0.001

Values are mean ± SD. *Test for comparison of FD-OCT versus IVUS was by paired *t* test.
FD-OCT = frequency-domain optical coherence tomography; IVUS = intravascular ultrasound.

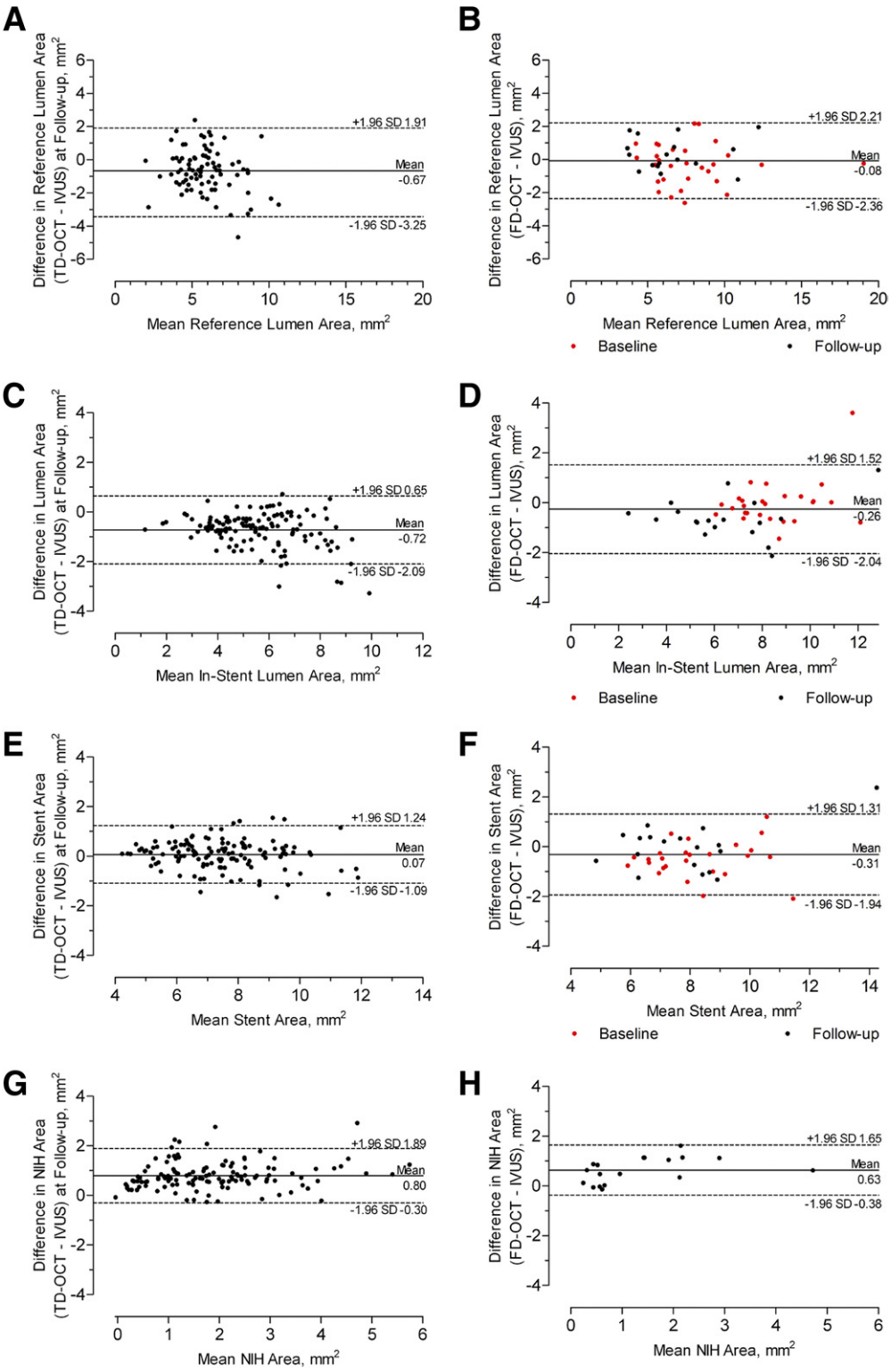

Figure 2. Bland-Altman Plots of OCT and IVUS Measurements in Stented Vessels

Comparison of stented region measurements evaluated by TD-OCT and FD-OCT versus IVUS. Bland-Altman plots for reference lumen area **(A and B)**, in-stent lumen area **(C and D)**, stent area **(E and F)**, and neointimal hyperplasia (NIH) **(G and H)** are represented. Abbreviations as in Figure 1.

Table 3. FD-OCT Versus IVUS Assessment of Stented Vessels Post PCI and at Follow-Up

	Baseline				Follow-Up			
	IVUS (n = 26)	FD-OCT (n = 26)	Difference (OCT—IVUS) (n = 26)	p Value	IVUS (n = 18)	FD-OCT (n = 18)	Difference (OCT—IVUS) (n = 18)	p Value
Mean reference lumen area, mm^2*	7.83 ± 2.95	7.52 ± 2.92	−0.31 ± 1.21	0.333	6.38 ± 2.60	6.72 ± 2.63	0.34 ± 0.98	0.070
Mean reference lumen diameter, mm*	3.10 ± 0.55	3.03 ± 0.54	−0.07 ± 0.25	0.281	2.77 ± 0.56	2.85 ± 0.53	0.08 ± 0.23	0.091
In-stent lumen area, mm^2								
Mean	8.52 ± 1.54	8.51 ± 1.83	−0.01 ± 0.90	0.946	6.80 ± 2.34	6.19 ± 2.48	−0.61 ± 0.81	0.005
Min	6.37 ± 1.40	6.51 ± 1.72	0.14 ± 1.12	0.541	4.38 ± 2.01	3.39 ± 1.89	−1.00 ± 0.80	<0.001
Max	11.00 ± 3.53	10.73 ± 3.00	−0.27 ± 1.56	0.382	8.65 ± 2.71	8.69 ± 3.08	0.04 ± 1.85	0.926
Stent area, mm^2								
Mean	8.52 ± 1.54	8.02 ± 1.61	−0.50 ± 0.73	0.002	7.82 ± 1.89	7.78 ± 2.27	−0.04 ± 0.91	0.854
Min	6.37 ± 1.40	6.24 ± 1.66	−0.13 ± 1.18	0.573	6.23 ± 1.47	6.00 ± 1.64	−0.23 ± 0.75	0.216
Max	11.00 ± 3.53	9.53 ± 1.89	−1.46 ± 2.39	0.005	9.44 ± 2.34	9.62 ± 2.91	0.18 ± 1.67	0.658
NIH area, mm^2†	—	—	—	—	1.03 ± 1.08	1.66 ± 1.30	0.63 ± 0.52	<0.001
Protruding area, mm^2	0.00 ± 0.00	0.16 ± 0.07	0.16 ± 0.07	<0.001	—	—	—	—
Stenosis (%)‡	—	—	—	—	14.13 ± 15.40	22.00 ± 17.58	7.87 ± 6.03	<0.001
Malapposition area, mm^2	0.00 ± 0.01	0.24 ± 0.48	0.24 ± 0.48	0.017	0.01 ± 0.05	0.06 ± 0.08	0.04 ± 0.07	0.010

Values are mean ± SD. *The number of reference edges: n = 30 for baseline and n = 17 for follow-up. †NIH area was computed as; (stent area − lumen area + malapposition area). ‡Stenosis was computed as; NIH area × 100/stent area.

NIH = neointimal hyperplasia; PCI = percutaneous coronary intervention; other abbreviations as in Table 1.

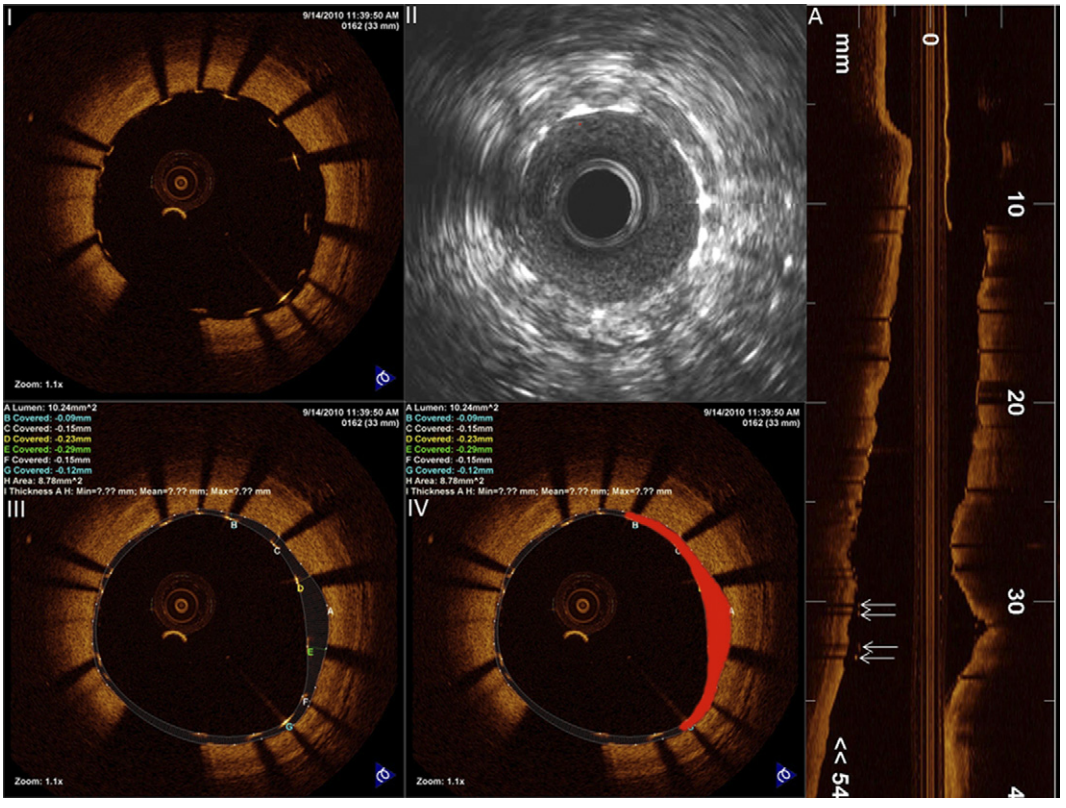

Figure 3. Stent Strut Malapposition Assessments by IVUS and OCT

A longitudinal view of OCT in a stented segment is represented in **A**, which shows malapposed stent struts in the proximal part **(white solid arrows)**. Cross-sections **I and II** correspond to the same regions in the OCT and IVUS evaluations, respectively, coregistered using side branches as landmarks. Malapposed stent struts are clearly revealed by OCT, whereas malapposition is not suspected by IVUS. OCT enables strut-level assessment of malapposition **(III)**, as well as the measurement of the area of malapposition (**IV**, rendered in **red**). Abbreviations as in Figure 1.

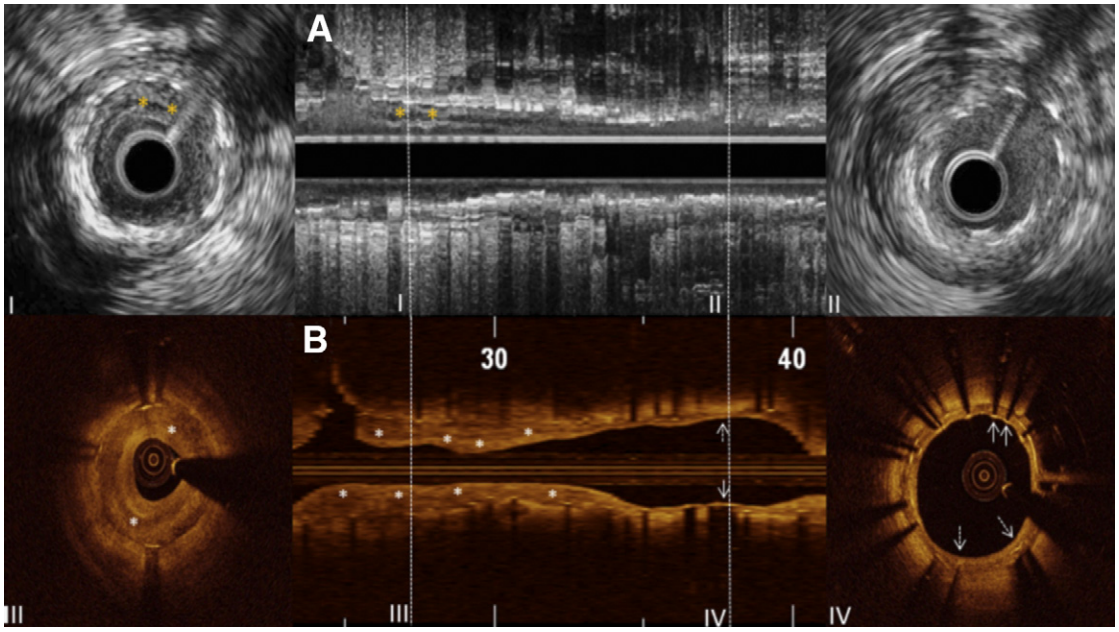

Figure 4. Evaluation of NIH by IVUS and OCT.

In **(A, center panel)**, a longitudinal IVUS view of a stented segment reveals a region with intrastent neointimal hyperplasia (NIH) **(yellow asterisks)**, which can be better depicted in the cross-sectional view represented in **I**. In **II**, the presence of NIH is not shown by IVUS (the struts would be considered uncovered by this method). The same region, coregistered using side branches as landmarks, is represented in the OCT longitudinal view **(B, center panel)**. Exacerbated NIH **(white asterisks)** in the mid-distal part of the stent is shown in **III**, and less exacerbated NIH in the proximal part of the stent (**white solid arrows** indicate struts covered by a thin NIH, and **white dashed arrows** highlight a slightly thicker NIH covering the stent struts is well depicted in the cross-sectional view shown in **IV**. Abbreviations as in Figure 1.

Both clinicians and investigators should be aware of fundamental differences between TD- and FD-OCT technologies that may impact image acquisition and interpretation. Although FD-OCT improved image quality compared with prior-generation TD-OCT (A-lines/frame: 500 to 1,000 vs. 200, respectively), it appears to be the method and speed of image acquisition that best distinguish these technologies. Briefly, TD-OCT acquires intravascular images at 1- to 3-mm/s pull back speed during vessel occlusion and concomitant intracoronary infusion of saline at 0.5 to 1 ml/s. Nonocclusive FD-OCT imaging is acquired during a 3- to 5-mm/s intracoronary infusion of nondiluted iodine contrast during high-speed pull back (20 to 25 mm/s) (14). The impact of vessel occlusion becomes evident in native coronary arteries and reference segments of stented vessels, as shown in this study, because these segments are susceptible to changes in intracoronary flow and pressure leading to smaller dimensions detected by TD-OCT. By contrast, the fact that reference lumen dimensions were equivalent between IVUS and FD-OCT is reassuring for clinicians using this new technology to determine device size during PCI in routine practice.

Coronary disease severity in native arteries was more significant by FD-OCT compared with IVUS (Table 2). A recent first-in-man safety and feasibility evaluation of optical frequency-domain imaging (Terumo Intravascular OFDI system, Terumo Corporation, Tokyo, Japan) observed similar findings (18). Whether such discrepancies represent underestimation of disease severity by IVUS or overestimation by OCT is difficult to prove. Such differences between light and ultrasound image formation and quantification were not observed in our in vitro study (12), and one can only speculate on possible explanations for the observed differences in vivo: 1) sharper delineation of the lumen–wall interface coupled with smooth longitudinal lumen visualization by FD-OCT may allow more precise identification of the site of MLA when compared to IVUS; 2) although faster pull back provides smoother longitudinal views, it may preclude selection of frames at maximum diastole in FD-OCT images; and 3) the smaller profile of the FD-OCT catheter when compared with IVUS may cause less stretch (Dotter effect) of the vessel in high-grade stenoses. Independent of the mechanisms, clinicians should be aware of the differences in MLA measurements observed in the present study and refrain from using IVUS-based thresholds to define coronary disease severity by OCT. Future studies are required to define OCT-based appropriateness criteria to indicate PCI (19).

Post-PCI stent area has long been associated with restenosis and thrombosis (4,20,21) Although follow-up stent

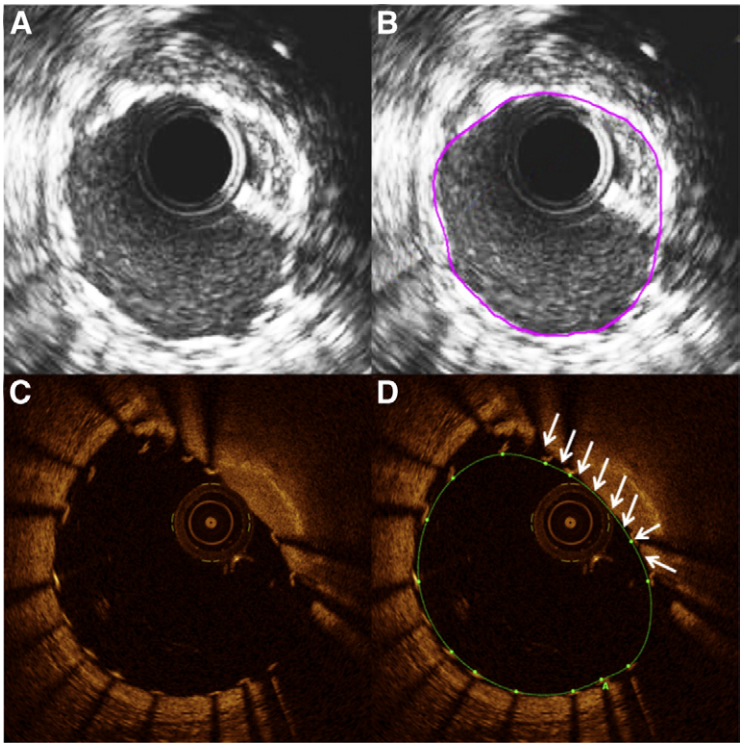

Figure 5. Stent Area Overestimation by IVUS in a Highly Calcified Plaque

(A) IVUS cross section of an eccentric calcified plaque treated with a stent. Stent area is measured in **(B)** (**purple contour**, 6.53 mm^2). Note that due to the presence of calcium from 12 to 4 o'clock, it is difficult to accurately trace the stent contour. **(C)** The coregistered image visualized by FD-OCT reveals the presence of calcium without artifacts. Stent area is measured accurately (**green contour**, 5.96 mm^2). **White arrows** in the calcified region indicate the difficulty in obtaining uniform stent expansion. Abbreviations as in Figure 1.

area measurements were similar among methods, the post-procedure stent area was larger by IVUS compared with FD-OCT. These somewhat unexpected results led to a detailed review of images and measurements by 1 additional senior analyst in our group, who validated the assessments. A higher proportion of calcification was observed in the population with post-PCI imaging compared with follow-up cases (85% post-PCI frames had some degree of calcification vs. 22% at follow-up). We hypothesized that this may have affected detection of the stent–luminal interface on post-procedure IVUS images because of blooming artifacts from both stent and calcium reflections (Fig. 5). Although stent struts also generate blooming artifact on OCT images (14), calcium does not (22). Therefore, the stent–lumen interface could be delineated by FD-OCT even in calcified plaques (Fig. 5). This phenomenon may also help to explain the observation of higher volumes of malapposition detected by FD-OCT and similar intrastent lumen areas despite smaller stent areas and higher tissue protrusion. Future studies are required to investigate whether more accurate detection of post-procedure stent area in calcified vessels by FD-OCT is clinically relevant.

Stent malapposition has been associated with late and very late stent thrombosis (23). Prior studies have shown better accuracy of TD-OCT to detect stent malapposition compared with IVUS (24,25). Similarly, prior studies have shown better accuracy of TD-OCT to detect NIH (26). Our findings expand upon these observations by demonstrating superior detection of malapposition and NIH by FD-OCT, which was more pronounced at lower degrees of tissue proliferation (Online Fig. 1) (26). We attributed the high sensitivity of OCT to its superior spatial resolution and imaging acquisition in a virtually blood-free environment, resulting in high contrast between the lumen and vessel wall interface.

Taken together, the present data suggest superior accuracy and sensitivity of FD-OCT assessments of native coronary disease and PCI compared with IVUS; however, studies evaluating patients' outcomes are needed to comprehensively understand the clinical value of FD-OCT. Physicians utilizing these intravascular imaging technologies in routine clinical practice should be cognizant of the significant differences in measurements of native coronary artery disease and stented vessels between the methods.

JACC: CARDIOVASCULAR INTERVENTIONS, VOL. 6, NO. 3, 2013
MARCH 2013:228–36

Study limitations. The study did not include comparisons between TD-OCT versus IVUS in native coronary arteries, which has been performed previously (10). In addition, no comparisons between TD- and FD-OCT were performed, as they were used in different populations.

Intrinsic differences between methods (pull back speed, lateral resolution, frame rate, and so on) preclude frame-level coregistration. In the present study, image analysis was performed in all frames (i.e., every 0.2 mm) in nonstented coronaries or every 1 mm in stented vessels, and most comparisons involve mean area measurements along the entire target segment (27), minimizing the impact of single cross-sectional metrics. However, we cannot rule out the possibility that cross-sectional image selection may explain some of the differences observed in MLA measurements. It is, nevertheless, important to note that accurate selection of the site of MLA is a critical step in the process of disease assessment in clinical practice.

Reprint requests and correspondence: Dr. Marco A. Costa, Harrington Heart and Vascular Institute, University Hospitals Case Medical Center, Case Western Reserve University, 11100 Euclid Avenue, Lakeside 3113, Mailstop LKS 5038 Cleveland, Ohio 44106. E-mail: marco.costa@uhhospitals.org.

REFERENCES

1. Colombo A, Hall P, Nakamura S, et al. Intracoronary stenting without anticoagulation accomplished with intravascular ultrasound guidance. Circulation 1995;91:1676–88.
2. Moussa I, Moses J, Di Mario C, et al. Does the specific intravascular ultrasound criterion used to optimize stent expansion have an impact on the probability of stent restenosis? Am J Cardiol 1999;83:1012–7.
3. Russo RJ, Silva PD, Teirstein PS, et al. A randomized controlled trial of angiography versus intravascular ultrasound-directed bare-metal coronary stent placement (the AVID trial). Circ Cardiovasc Interv 2009;2:113–23.
4. Doi H, Maehara A, Mintz GS, et al. Impact of post-intervention minimal stent area on 9-month follow-up patency of paclitaxel-eluting stents: an integrated intravascular ultrasound analysis from the Taxus IV, V, and VI and TAXUS ATLAS Workhorse, Long Lesion, and Direct Stent trials. J Am Coll Cardiol Intv 2009;2:1269–75.
5. Jiménez-Quevedo P, Sabaté M, Angiolillo DJ, et al. Vascular effects of sirolimus-eluting versus bare-metal stents in diabetic patients: three-dimensional ultrasound results of the Diabetes and Sirolimus-Eluting Stent (DIABETES) trial. J Am Coll Cardiol 2006;47:2172–9.
6. Nissen SE, Gurley JC, Grines CL, et al. Intravascular ultrasound assessment of lumen size and wall morphology in normal subjects and patients with coronary artery disease. Circulation 1991;84:1087–99.
7. Hoffmann R, Haager P, Mintz GS, et al. The impact of high pressure vs low pressure stent implantation on intimal hyperplasia and follow-up lumen dimensions; results of a randomized trial. Eur Heart J 2001;22:2015–24.
8. Sousa JE, Costa MA, Sousa AG, et al. Two-year angiographic and intravascular ultrasound follow-up after implantation of sirolimus-eluting stents in human coronary arteries. Circulation 2003;107:381–3.
9. Suzuki Y, Ikeno F, Koizumi T, et al. In vivo comparison between optical coherence tomography and intravascular ultrasound for detecting small degrees of in-stent neointima after stent implantation. J Am Coll Cardiol Intv 2008;1:168–73.
10. Gonzalo N, Serruys PW, García-García HM, et al. Quantitative ex vivo and in vivo comparison of lumen dimensions measured by optical coherence tomography and intravascular ultrasound in human coronary arteries. Rev Esp Cardiol 2009;62:615–24.
11. Takarada S, Imanishi T, Liu Y, et al. Advantage of next-generation frequency-domain optical coherence tomography compared with conventional time-domain system in the assessment of coronary lesion. Catheter Cardiovasc Interv 2010;75:202–6.
12. Tahara S, Bezerra HG, Baibars M, et al. In vitro validation of new Fourier-domain optical coherence tomography. EuroIntervention 2011;6:875–82.
13. Guagliumi G, Sirbu V. Optical coherence tomography: high resolution intravascular imaging to evaluate vascular healing after coronary stenting. Catheter Cardiovasc Interv 2008;72:237–47.
14. Bezerra H, Costa M, Guagliumi G, Rollins A, Simon D. Intracoronary optical coherence tomography: a comprehensive review: clinical and research applications. J Am Coll Cardiol Intv 2009;2:1035–46.
15. Guagliumi G, Musumeci G, Sirbu V, et al. Optical coherence tomography assessment of in vivo vascular response after implantation of overlapping bare-metal and drug-eluting stents. J Am Coll Cardiol Intv 2010;3:531–9.
16. Bouma BE, Tearney GJ, Yabushita H, et al. Evaluation of intracoronary stenting by intravascular optical coherence tomography. Heart 2003;89:317–20.
17. Gonzalo N, Garcia-Garcia HM, Serruys PW, et al. Reproducibility of quantitative optical coherence tomography for stent analysis. EuroIntervention 2009;5:224–32.
18. Okamura T, Onuma Y, García-García HM, et al. First-in-man evaluation of intravascular optical frequency-domain imaging (OFDI) of Terumo: a comparison with intravascular ultrasound and quantitative coronary angiography. EuroIntervention 2011;6:1037–45.
19. Marso S, Terstein P, Kereiakes D, Moses J, Lasala J, Grantham A. Percutaneous coronary intervention use in the United States: defining measures of appropriateness. J Am Coll Cardiol Intv 2012;5:229–35.
20. Sonoda S, Morino Y, Ako J, et al. Impact of final stent dimensions on long-term results following sirolimus-eluting stent implantation: serial intravascular ultrasound analysis from the SIRIUS trial. J Am Coll Cardiol 2004;43:1959–63.
21. Cheneau E, Leborgne L, Mintz GS, et al. Predictors of subacute stent thrombosis: results of a systematic intravascular ultrasound study. Circulation 2003;108:43–7.
22. Kume T, Okura H, Kawamoto T, et al. Assessment of the coronary calcification by optical coherence tomography. EuroIntervention 2011;6:768–72.
23. Hassan A, Bergheanu S, Stijnen T, et al. Late stent malapposition risk is higher after drug-eluting stent compared with bare-metal stent implantation and associates with late stent thrombosis. Eur Heart J 2012;31:1172–80.
24. Ozaki Y, Okumura M, Ismail TF, et al. The fate of incomplete stent apposition with drug-eluting stents: an optical coherence tomography-based natural history study. Eur Heart J 2010;31:1470–6.
25. Gutiérrez-Chico JL, Wykrzykowska J, Nüesch E, et al. Vascular tissue reaction to acute malapposition in human coronary arteries: sequential assessment with optical coherence tomography. Circ Cardiovasc Interv 2012;5:20–9, S1–8.
26. Matsumoto D, Shite J, Shinke T, et al. Neointimal coverage of sirolimus-eluting stents at 6-month follow-up: evaluated by optical coherence tomography. Eur Heart J 2007;28:961–967.26.
27. Mehanna EA, Attizzani GF, Kyono H, Hake M, Bezerra HG. Assessment of coronary stent by optical coherence tomography, methodology and definitions. Int J Cardiovasc Imaging 2011;27:259–69.

Key Words: intravascular ultrasound ■ optical coherence tomography ■ percutaneous coronary intervention.

APPENDIX

For supplementary figures and tables, please see the online version of this paper.